

Magnetic switching of ferromagnetic nanotubes

R. Sharif,^{1,a)} S. Shamaila,¹ M. Ma,¹ L. D. Yao,¹ R. C. Yu,¹ X. F. Han,^{1,b)} and M. Khaleeq-ur-Rahman²

¹Beijing National Laboratory for Condensed Matter Physics, Institute of Physics, Chinese Academy of Science, Beijing 100080, People's Republic of China

²Physics Department, University of Engineering and Technology, Lahore-54890, Pakistan

(Received 12 October 2007; accepted 31 December 2007; published online 24 January 2008)

The magnetic switching of ferromagnetic nanotubes as function of geometrical parameters has been investigated. The modes of magnetization reversal are observed to depend on the geometry of the nanotubes. Time dependent magnetization properties reveal that the nanotubes have strong magnetic viscosity effects. The values of magnetic viscosity coefficient (S) for different applied fields are high near the coercive field. © 2008 American Institute of Physics. [DOI: 10.1063/1.2836272]

During the last decade, interesting properties of magnetic nanowires have attracted much attention. Besides their interesting basic properties, there is evidence that they can be used in the fabrication of new nanodevices. Recently, magnetic nanotubes have been fabricated¹⁻⁴ and have become a symbol of new and fast developing research area of nanotechnology because of their technological applications in magnetic biotechnology.^{5,6} From theoretical point of view, tube geometry has advantages over wire geometry because it completely avoids a problem of mathematical singularity in micromagnetic distribution leading to uniform switching fields. Geometrically, magnetic nanotubes are characterized by their external and internal radii R and a , respectively, height (or length) H , and thickness $t=R-a$, where $a=0$ gives a solid cylinder geometry (wires) and $t>0$ gives a hollow cylinder geometry (tubes). Although the reversal process has been extensively studied for ferromagnetic nanowires,⁷⁻¹¹ the equivalent phenomenon in nanotubes has been poorly explored so far in spite of some potential advantages over solid cylinders. Since coercivity is important ferromagnetic material property and the complex role played by coercivity mechanism in magnetization reversal remains to be clarified for decades, many researchers still use it as a phenomenological rule. Two possible modes of magnetization reversal, uniform (coherent) and curling modes, have been discussed for ferromagnetic cylinders.^{12,13} The two magnetization reversal modes would give different angular dependences of coercivity, so the measurements of coercivity [$H_C(\theta)$] and remanent squareness [$SQ(\theta)$] curves (where θ is the angle between the applied field and long axis of the tubes) would provide helpful information about the reversal mechanisms.^{14,15} The shapes of $H_C(\theta)$ curves are determined by the magnetization reversal mechanism, where the $SQ(\theta)$ curves change as the overall easy axis of the nanotubes changes. Moreover, the time dependence of magnetization $M(t)$ would show strong magnetic viscosity effect due to thermally activated magnetization reversal mechanism for ferromagnetic cylinders.¹⁶ The rigorous analysis of reversal modes for a ferromagnetic hollow cylinder shows that magnetization reversal is influenced by the ratio of internal to external radii or thickness of the cylinder.¹³

In this letter, we will present the experimental results regarding the measurements of $H_C(\theta)$ and $SQ(\theta)$ curves for various ferromagnetic nanotubes (Co, Fe, Ni) electrodeposited in track etched polycarbonate membranes and study how the changes in thickness of the nanotubes change the shapes of $H_C(\theta)$ and $SQ(\theta)$ curves. We also measured the time dependent magnetization properties for Co nanotubes at different applied fields and calculated the magnetic viscosity coefficient. For present report, track etched polycarbonate membranes with pore size of ~ 600 nm and porosity of $\sim 10^6$ are selected for fabrication of magnetic nanotubes by dc electrodeposition. A thin gold layer is sputtered on one side of the membranes to serve as working electrode. The magnetic metals are preferentially deposited on the gold layer along the pore walls. The thickness of gold layer is varied to get the thicknesses $t_1 \sim 50$ nm and $t_2 \sim 150$ nm of the nanotube arrays. The electrolytes contain the desired metals in appropriate ratios and 40 g/l boric acid as buffer agent. The same lengths of the nanotubes are obtained by adjusting the time of electrodeposition such that the deposition is stopped as soon as the nanotubes emerge from the surface of the membrane. Therefore, the length of the nanotubes is $6 \mu\text{m}$ equal to the thickness of polycarbonate membranes. The morphology and structural properties are observed using field emission scanning electron microscopy (FESEM) and transmission electron microscopy (TEM). For TEM analysis, the samples are dissolved in chloroform. For magnetic time dependent measurements of Co nanotubes of thickness t_2 , the temperature is fixed at 300 K, and the sample is saturated with a positive applied field, then the desired negative reversed field is set and held constant, and the magnetization decay measurements $M(t)$ are taken for thousands of seconds. Magnetic properties are investigated using vibrating sample magnetometer and superconducting quantum interferometer device.

Figure 1(a) shows the FESEM images of Co nanotube arrays of thickness t_2 . The nanotubes of thickness $t_1 \sim 50$ nm are too thin to be observed from FESEM, so the samples are dissolved and then observed using TEM. Figure 1(b) shows the TEM images of the Co nanotubes. The inset of Fig. 1(b) is the diffraction pattern of nanotubes showing its fcc crystalline structure. Figure 2 shows the angular dependence of H_C for Co, Fe, and Ni nanotubes arrays (a) for thickness t_1 and (b) for t_2 . Figure 3 shows the angular dependence of remanence squareness (SQ) for Co, Fe, and Ni

^{a)}Electronic mail: rsharif2002@yahoo.com.

^{b)}Author to whom correspondence should be addressed. Electronic mail: xfhan@aphy.iphy.ac.cn.

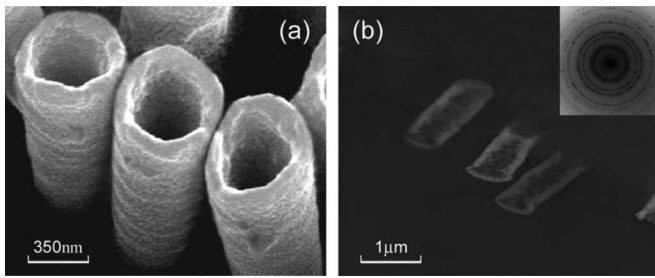


FIG. 1. Morphology of Co nanotubes: (a) FESEM images of Co nanotube arrays of thickness t_1 and (b) TEM images of Co nanotubes of thickness t_2 . The inset shows diffraction pattern of the nanotubes showing its fcc crystal-line structure.

nanotubes arrays (a) for thickness t_1 and (b) for t_2 . From Fig. 2(a), it is obvious that coercivity H_C of all the nanotube arrays with thickness t_1 first increases with angle and then decreases for higher angles up to $\theta = \pm 90^\circ$ representing an M -type variation. Similar behavior of $H_C(\theta)$ curves has already been observed for Ni nanowires.¹⁴ Figure 2(b) shows that coercivity H_C of Co, Ni, and Fe nanotubes of thickness t_2 increases with increasing angle (θ) from 0° to $\pm 90^\circ$. Such behavior has also been observed for Co, NiFe, and CoNiFe nanowires.¹⁴

For nanostructures, such as nanospheres and nanowires, there is a transition in the magnetization reversal mode from coherent to curling when the radius R exceeds a certain value. However, in nanotubes, this transition occurs at very small tube radius.¹⁷ The curling mode of magnetization reversal in an infinite cylinder predicts that H_C increases as angle (θ) increases having lowest H_C value at $\theta=0^\circ$ and highest value at $\theta = \pm 90^\circ$. Whereas the coherent rotation mode gives the highest and lowest H_C values for $\theta=0^\circ$ and $\theta = \pm 90^\circ$, respectively, i.e., H_C decreases as angle increases from 0° to $\pm 90^\circ$.^{14,15}

For the present work, the observed behavior of $H_C(\theta)$ for thickness t_2 [Fig. 2(b)] represents that the magnetization is

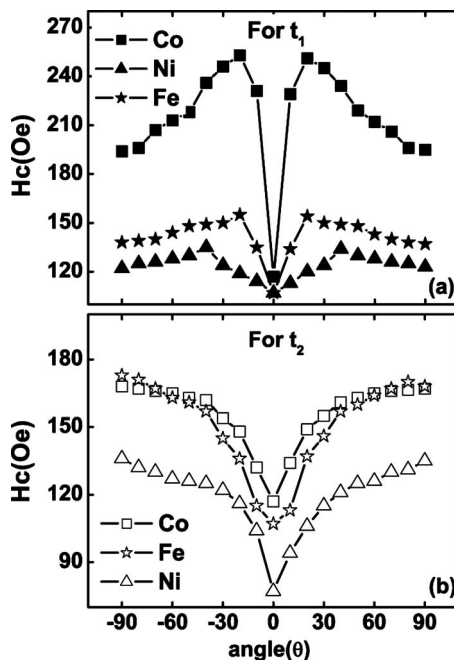


FIG. 2. Angular dependence of H_C for Co, Fe, and Ni nanotube arrays (a) for thickness t_1 and (b) for t_2 .

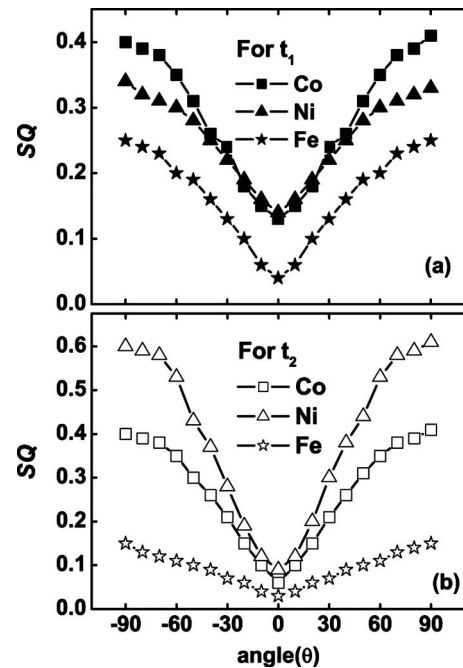


FIG. 3. Angular dependence of SQ for Co, Fe, and Ni nanotube arrays (a) for thickness t_1 and (b) for t_2 .

mainly determined by curling. Whereas the M -type variation for thickness t_1 [Fig. 2(a)] represents that at large angles, coherent rotation is dominant, while the curling happens for small angles ($\theta \leq \pm 40^\circ$). Since the outer diameter of the nanotubes considered here is large (~ 600 nm), so the expected curling rotation is obtained for thickness t_2 . For thickness t_1 , M -type behavior of $H_C(\theta)$ is due to the different alignments of magnetic moments with the applied field. The geometry of the nanotubes presents two characteristic ideal internal configurations according to their magnetization: parallel to the tube axis and concentric to the tube axis. The latter is the vortex state, where magnetic moments lay parallel to tube basis and circulate around its axis. Daub *et al.* presented that a vortex state for the larger diameter nanotubes is preferable.³ For our samples, the diameter of the nanotubes is 600 nm that is large enough to be concluded that the vortex mode is the most favorable state. The shapes of $SQ(\theta)$ curves are determined according to the easy axis of the arrays. It can be noted from Figs. 3(a) and 3(b) that SQ values for all nanotube arrays of thicknesses t_1 and t_2 increase with increase in angle having highest value at $\theta = \pm 90^\circ$ which is the easy axis of the arrays, as observed from the magnetization curves (not shown here). The magnetization reversal from coherent to curling over an energy barrier also appears due to thermal fluctuations.¹³ If these effects are taken into account, the magnetization is expected to vary exponentially with time $M(t) = M(0)e^{t/\tau}$, where $\tau = \tau_0 e^{-\Delta E/k_B T}$. The exponential time dependence of magnetization is due to one height of energy barrier. However, in real systems this exponential behavior is seldom observed due to different energy barriers coming from the distribution of the anisotropy and size.¹⁸

Figure 4(a) illustrates the time dependence of magnetization $M(t)$ for the Co nanotube arrays with the tube thickness of 150 nm at 300 K in different fields. It appears that the magnetization has logarithmic time dependence, exhibiting a typical relaxation behavior. Since magnetic relaxation

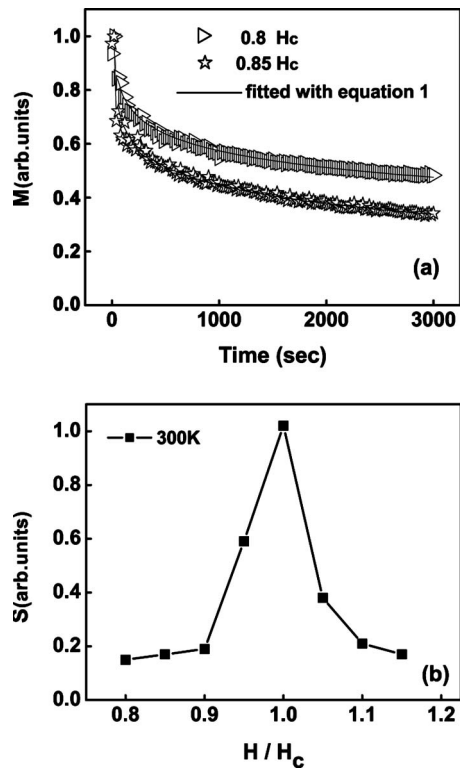


FIG. 4. (a) Time dependence of the magnetization $M(t)$ at 300 K with different applied fields for the Co nanotube arrays with thickness t_2 . (b) Field dependence of magnetic viscosity coefficients S for the Co nanotube arrays with thickness t_2 at 300 K.

is significant around H_C so the applied fields are 0.8, 0.85, 0.90, 0.95 Hc, and so on. Whereas 0.8 and 0.85 Hc are selected as an example to plot in Fig. 4(a). The observed time dependence of magnetization shows logarithmic behavior represented by the following equation:

$$M(t) = M_0[1 - S(H, T) \ln t], \quad (1)$$

where $S(H, T)$ is magnetic viscosity coefficients which can be obtained by fitting the above equation for time dependence of magnetization.¹⁸ For Co nanotube arrays of thickness t_2 , the magnetic viscosity coefficients $S(H, T)$ are determined by fitting Eq. (1). $S(H, T)$ values are plotted versus H/H_C which presents that the peak value of $S(H, T)$ is near

the coercive field H_C , as shown in Fig. 4(b). The behavior of $S(H, T)$ shows that the nanotubes have strong magnetic viscosity effects and that magnetization switching occurs near the coercive field H_C .

In summary, we have observed magnetic switching properties of ferromagnetic nanotubes by varying the thickness of nanotubes. Time dependent magnetic properties show that the nanotubes have strong magnetic viscosity effects. Due to thermal fluctuations, magnetization switching occurs near the coercive field (H_C).

The project was supported by the State Key Project of Fundamental Research of Ministry of Science and Technology (MOST, No. 2006CB932200). X. F. Han thanks the partial support of National Natural Science Foundation (NSFC Nos. 10574156, 50325104, 50528101, and 50721001). The authors R. Sharif and S. Shamaila are on study leave from University of Engineering and Technology, Lahore, Pakistan.

¹K. Nielsch, F. J. Castaño, C. A. Ross, and R. Krishnan, *J. Appl. Phys.* **98**, 034318 (2005).

²K. Nielsch, F. J. Castaño, S. Matthias, W. Lee, and C. A. Ross, *Adv. Eng. Mater.* **7**, 217 (2005).

³M. Daub, M. Knez, U. Gösele, and K. Nielsch, *J. Appl. Phys.* **101**, 09J111 (2007).

⁴Z. K. Wang, H. S. Lim, H. Y. Liu, S. C. Ng, M. H. Kuok, L. L. Tay, D. J. Lockwood, M. G. Cottam, K. L. Hobbs, P. R. Larson, J. C. Keay, G. D. Lian, and M. B. Johnson, *Phys. Rev. Lett.* **94**, 137208 (2005).

⁵A. K. Salem, P. C. Searson, and K. W. Leong, *Nat. Mater.* **2**, 668 (2003).

⁶C. C. Berry and A. S. G. Curtis, *J. Phys. D* **36**, R198 (2003).

⁷R. Varga, K. L. Garcia, M. Vázquez, and P. Vojtanik, *Phys. Rev. Lett.* **94**, 017201 (2005).

⁸D. Hinzke and U. Nowak, *J. Magn. Magn. Mater.* **221**, 365 (2000).

⁹H. Forster, T. Schrefl, D. Suess, W. Scholz, V. Tsiantos, R. Dittrich, and J. Fidler, *J. Appl. Phys.* **91**, 6914 (2002).

¹⁰R. Wieser, U. Nowak, and K. D. Usadel, *Phys. Rev. B* **69**, 064401 (2004).

¹¹K. Nielsch, R. Hertel, R. B. Wehrspohn, J. Barthel, J. Kirschner, U. Gösele, S. F. Fischer, and H. Kronmüller, *IEEE Trans. Magn.* **38**, 2571 (2002).

¹²A. Aharoni and S. Shtrikman, *Phys. Rev.* **109**, 1522 (1958).

¹³C.-R. Chang, C. M. Lee, and J.-S. Yang, *Phys. Rev. B* **50**, 6461 (1994).

¹⁴G. C. Han, B. Y. Zong, P. Luo, and Y. H. Wu, *J. Appl. Phys.* **93**, 9202 (2003).

¹⁵L. Sun, Y. Hao, C.-L. Chien, and P. C. Searson, *IBM J. Res. Dev.* **49**, 79 (2005).

¹⁶H.-B. Braun, *Phys. Rev. Lett.* **71**, 3557 (1993).

¹⁷Y. C. Sui, R. Skomski, K. D. Sorge, and D. J. Sellmyer, *Appl. Phys. Lett.* **84**, 1525 (2004).

¹⁸J.-E. Wegrowe, O. Fruchart, J.-P. Nozières, D. Givord, F. Rousseaux, D. Decanini, and J. Ph. Ansermet, *J. Appl. Phys.* **86**, 1028 (1999).